Acta Montanistica Slovaca
ISSN 1335-1788
actamont.tuke.sk

Estimation of Uncertainties in Determination of Natural Gas Thermodynamic Properties Based Upon In-situ Raman Analyses of Gas Mixtures

Karol M. DĄBROWSKI[1], Jan BARBACKI[1], Szymon KUCZYŃSKI[1], Rafał SMULSKI[1] and Stanisław NAGY[1]*

Authors' affiliations and addresses:
[1] AGH University of Science and Technology , al. Mickiewicza 30, 30-059 Krakow, POLAND
e-mail: karol.dabrowski@agh.edu.pl
e-mail: jan.barbacki@agh.edu.pl
e-mail: szymon.kuczynski@agh.edu.pl
e-mail:smulski@agh.edu.pl
e-mail: stanislaw.nagy@agh.edu.pl

***Correspondence:**
Karol M. Dąbrowski, AGH University of Science and Technology , al. Mickiewicza 30, 30-059 Krakow, POLAND
Tel. +48 12 617 22 90
karol.dabrowski@agh.edu.pl

Funding information:
National Centre for Research and Development and industrial partners, project no.: BG1/IRES/13

Acknowledgment:
The authors would like to acknowledge Mr. Michał Łaśko for the help in Raman measurements.

How to cite this article:
Dąbrowski, K. M., Barbacki, J., Kuczyński, S., Smulski, R. and Nagy, S. (2022). Estimation of Uncertainties in Determination of Natural Gas Thermodynamic Properties Based Upon In-situ Raman Analyses of Gas Mixtures. *Acta Montanistica Slovaca*. Volume 27 (1), 84-99

DOI:
https://doi.org/10.46544/AMS.v27i1.07

Abstract
Raman spectroscopy is used in a real-time determination of the thermodynamic properties of natural gas. Two methods of Raman signal analysis are discussed. The first method is an analytical algorithm based on linear regression, which utilizes peak area. The second is an Artificial Neural Network algorithm that can utilize both peak area and its position. A detailed discussion of presented approaches is shown on reference data obtained using specially designed setup Raman with 105 m long fiber optic probe and a high-pressure cell. The proposed analysis allowed the calculation of composition for any arbitrarily chosen pressure. The feasibility of this approach is shown by the determination of composition for a gas flow in a separator installation on a gas production well. Results are compared with gas chromatography which allows the uncertainty determination of the method.

Keywords
Raman spectroscopy, composition analysis, natural gas, artificial intelligence, machine learning

Introduction

Determination of natural gas composition plays a vital role in the Oil and Gas industry. Determining the composition of natural gas (also gas and condensate gas) is an essential issue in the process of exploration, documentation, and exploitation of gas and oil reservoirs. The problem of determining the composition of reservoir fluid is inherently connected with the problem of preparing the well and deposit for collecting a representative sample of reservoir fluid. The analysis of reservoir gas can be performed with the use of the downhole reservoir sampler or by analyzing gas in surface conditions from the separator. Determining composition is crucial to calculate thermodynamic properties, for example, heating Value, Wobbe Index, Compressibility Factor, gas density, gas viscosity, etc. The composition can be considered as a quality determinant in various technological processes such as production or separation (high-pressure separators) and process installations. Composition is commonly measured using gas chromatography (GC). However, it requires gas sampling, which limits its use in monitoring or performing in-situ experiments. Those downsides can be overcome by the use of Raman Spectroscopy (RS). However, the RS method requires calibration - usually based on gas chromatography.

This spectroscopy technique utilizes electromagnetic radiation. Incident monochromatic beam with a wavenumber ω_i passing through a material system can be scattered on a molecule. Angular frequency of scattered radiation is given ω_f. Interaction with a photon can trigger a transition from an initial energetic state of molecule denoted as E_i to a final state denoted E_f. Transition energy is given by $E_{fi} = E_f - E_i$ while transition angular frequency by $\omega_{fi} = \omega_f - \omega_i$ we can write $E_{fi} = \hbar\omega_{fi}$. Transition without a change of a scattered radiation angular frequency is a Rayleigh scattering, while with a change is a Raman scattering (Long, 2002). The transition of a molecule state can occur between rotational, vibrational levels. This results in appearance peaks in a spectrum. Those peaks are also called Raman bands. Since E_{fi} can be positive or negative Raman bands can have an angular frequency lower than the incident radiation $\omega_{fi} = \omega_f - |\omega_i|$ (Stokes bands) of higher $\omega_{fi} = \omega_f + |\omega_i|$ (anti-Stokes bands).

RS is widely used for qualitative measurements in pharmaceutical analysis (De Beer, 2011; Bērziņš, 2020), earth (Beyssac, 2020), or environmental science (Halvorson, 2010). Several works have focused on natural gas studies. Raman signal from high-pressure gaseousness hydrocarbon mixtures have been characterized (Hansen, 2000; Hansen, 2001a; Petrov, 2017; Kuczyński, 2017), and temperature influence have been discussed (Shang, 2014). Feasibility of determination of molar fraction for binary and multi-component samples has been shown (Kiefer, 2008a; Kiefer, 2008b; Kiefer, 2015; Buldakov, 2013; Petrov, 2016). Application in a biogas monitoring was presented (Eichmann, 2014; Sieburg, 2018). Wobbe Index determination method was shown in (Sandfort, 2017). Several techniques employing optical fiber in the natural gas analysis were developed (Hippler, 2015; Sieburg, 2019). RS was also used in measuring unconventional deposits such as shale or coal seams (Bryndzia et al., 2016) or coalbed reservoirs analysis (MacDonald, 2007).

In this paper, we will present a more generalized approach that enables the determination of molar fraction for wet gas under any high-pressure conditions based on peak analysis as well as based on wavenumber shift. This shift is linear for binary samples (Hansen, 2001b; Frosch, 2007; Petrov, 2019). We show that in the case of multi-component samples, this behavior is non-linear. Considering this shift enhances results compared to pure area peak analysis and in perspective in terms of two-phase fluid monitoring. The designed Raman setup utilizes a fiber optic probe which can provide real-time measurements in in-situ conditions. A detailed description of collected data processing will be shown. The pressure behavior of Raman spectra was determined based on linear regression. Preprocessed data were further used in composition calculation either using partial least squares regression procedure or Artificial Neural Network algorithm.

Partial least squares regression (PLS) is an analytical method widely used in approximation (Kutner, 2004) and spectra analysis (Lee, 2018). It can give robust results for the limited number of data but requires assumptions about linearity or at least local linearity (Montgomery, 2012). Therefore assumes a strictly defined relation between measured values.

An Artificial Neural Network stimulates the activity of brain cells. In contrast to the PLS method, ANN does not require any knowledge about the relation between input and output data. It is capable of building a non-linear model with many input variables (Gautam, 2015; Pan, 2021). However, it does not give direct access to the structure of the model, therefore sometimes troublesome validation of operation is necessary. Another challenge is the requirement of a large set of learning data, while in this studies our dataset is relatively small.

ANNs are typically used in categorization and qualitative analysis. Particularly for speech recognition and translation (Lippmann, 1987). The feasibility of quantitative analysis was also shown by several authors (Özmen, 2006; Goodacre, 1994) and in particular with the use of Raman spectroscopy (Özbalci, 2013). ANNs are also used in reservoir simulations (Zubarev, 2009; Al-Fattah, 2001), reservoir characterization (Korjani, 2016; Hegeman, 2009), gas list optimization (Ranjan, 2015), composition analysis (Briones, 1994; Al-Sirri, 2011), or bubble point determination (Al-Marhoun, 2014).

We will compare these two methods in terms of usability in natural gas sensing. A present detailed discussion of differences in both approaches shows their limitation and perspectives. We will show a practical application of this method by determining the molar fraction of gas using a specially constructed setup. The setup is equipped with a fiber-optic probe which increases its usability for an industrial application (Włodek, 2016; Dąbrowski, 2018). This sensing system can be a useful tool in various fields of the petrol industry, especially for real-time downhole monitoring (Dąbrowski, 2019).

Material and Methods

Raman system

The scheme of a constructed laboratory system is shown in Fig. 1. The main part is a portable Raman spectrometer in axial transmissive geometry. Equipped with a 105 m fiber optic probe. The intensity of a Raman signal for element i is given by (Kiefer, 2008):

$$I_i = k\Omega \frac{\partial \sigma_i}{\partial \Omega} \frac{N_i}{V} L I_0$$

where I_0 is incident beam intensity, k is geometry factor, Ω is collecting solid angle, σ_i is Raman cross-section for a given element, N_i is the number of molecules of component i in volume V and L is scattering volume since the Raman signal is of the order of 10^{-8} of incident radiation for liquids (Bowley, 2012) and 10^{-11} for gases. Therefore, high sensitive instrumentation is required.

For spectra collection, a Kaiser Raman Analyzer Rxn2 with fiber-coupled AirHead™ probe was used. It was equipped with a 785 nm diode laser with maximal power 400 mW, f/1.8 focusing lens, 4 cm^{-1} resolution. The probe was fixed-focus with <1 mm focal length and 50 μm spot size. Proper choice of a source was crucial in terms of planned experiments. Raman scattering cross-section is proportional to λ^{-4}, where λ is a laser wavelength (Bowley, 2012). Compared to the Nd-Yag 532 nm source, intensity for the longer wavelength decreases of the order of 5 dB. On the other hand, shorter wavelengths are stronger attenuated in a fiber optic. Attenuation factors for used multimode fiberoptic are of the order of 5 for 785 and 20 dB for 532 nm laser. For 105 m long fiber, it causes an intensity drop of 12 % and 39 %, respectively, while for 1 km fiber, this drop is 70 % and 99 %. This shows that a source with a shorter wavelength cannot be used in perspective for downhole measurements. Source 1064 nm could have the smallest attenuation, but current detectors require liquid nitrogen cooling, which makes in-situ measurements troublesome.

Radiation was measured by a Charge-Coupled Device (CCD) detector. The sensor had 1024x256 pixels of the size of 26x26 μm and was cooled by Peltier thermoelectric device to -40°C. Spectrum was recorded for a wavenumber range from 150 cm^{-1} to 3450 cm^{-1}.

The laser beam travels along with the multimode optical fiber to a probe that focuses the beam onto the sample. Backscattered radiation is collimated and travels to the spectrometer by another fiber. For convenience, these two fibers were put in one cable braid. Depending on the application, different lengths of fiber can be used up to 1-2 km. However, in current studies, we limited the length to 105 m.

The probe was mounted to high pressure and high temperature (HPHT) cell, which simulated in-situ conditions for measurements. The total accumulation time of a single spectrum was 2 minutes. Since no sampling is required, this is also a repetition time for subsequent measurements. Recommended conditioning time of a well is 12-24 hours with 30 min intervals between which flow is lowering (API RP44, 2004). Therefore, the presented method allows real-time measurements. A total of 8 different mixtures were measured to build a spectra database. Concentrations varied between 43.30-100 % for CH_4, 0-14.27 % for C_2H_6, 0-9.65 %-C_3H_8, 0-2.46 %- i-C_4H_{10}, 1.94% n-C_4H_{10} and 0-46.10% N_2, while minimal concentrations were: 43.30% for CH_4, 4.01% for C_2H_6, 1.94%-C_3H_8, 0.73%- i-C_4H_{10}, 0.48% n-C_4H_{10} and 0.46% N_2. Another mixture was used as a test sample to show the feasibility of the method and determine its uncertainties.

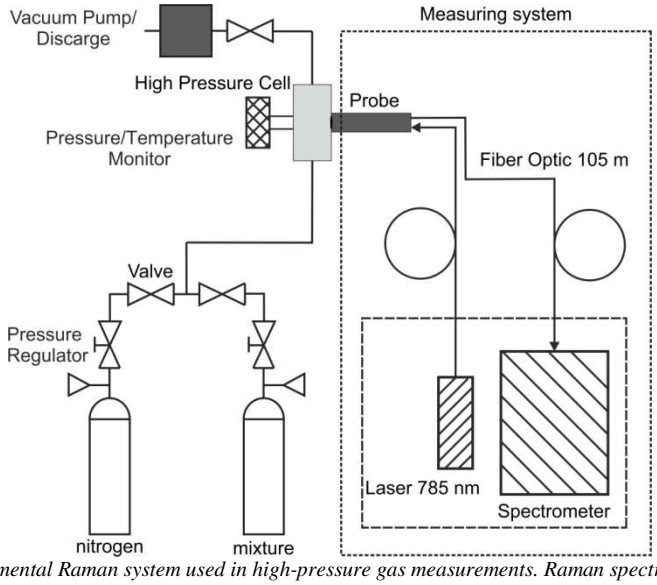

Fig. 1. Scheme of an experimental Raman system used in high-pressure gas measurements. Raman spectrometer was equipped with a 785 nm laser. Incident beam and scattered radiation travel along 105 m fiber optic. Probe for laboratory measurements was mounted into a high-pressure, high-temperature cell. Gases were supplied directly from gas cylinders. The pressure was regulated manually by a pressure reducer.

Gas chromatography equipment

For validation of composition determination, Gas Chromatography (GC) was used. The GC instrument was an Agilent Model 6890 Gas Chromatograph. The system consisted of the following components: 6-port sample valve with 0.25 cc sample loop, capillary split/splitless injector with EPC, porous polymer capillary column PLOT-Q (30 m x0.53 mm x 0.4 microns), thermal conductivity detector (TCD) with EPC. Helium and air used for the GC and TCD were high purity (99.9995 % v/v) gases. Helium was used at a constant flow of 6.9 mL/min, and other flow rates were maintained by using electronic flow control. An injection port was in a split mode (1:15 split ratio) and held at 250°C. A temperature program consisted of the oven being initially set to a temperature of 60°C and held for 5 min, and then ramped at 20°C/min to 200°C, where a temperature was held for 1 min, thereby resulting in a total run time of 13 min. The TCD was held at 250°C. To determine the precision of a GC Relative Standard Deviation (RSD) by measuring signal from the gas-certified mixture was calculated. RSD is given by (Zuas, 2016):

$$\boldsymbol{RSD} = \frac{\boldsymbol{100}}{\boldsymbol{\bar{y}}} \sqrt{\sum_{\boldsymbol{i}} \frac{(\boldsymbol{y_i} - \boldsymbol{\bar{y}})^2}{\boldsymbol{n-1}}}$$

where y_i is peak area of a given component, $\bar{y}$ is the average area of the component, n number of runs.

Overview of the algorithm

Concentration determination of unknown samples was performed using a designed procedure. A Diagram of a building program is shown in Fig. 2. In this paper, we show its application for gas measurements, but it can be used without modifications also for liquids. The algorithm has several steps. It can be divided into two main parts.

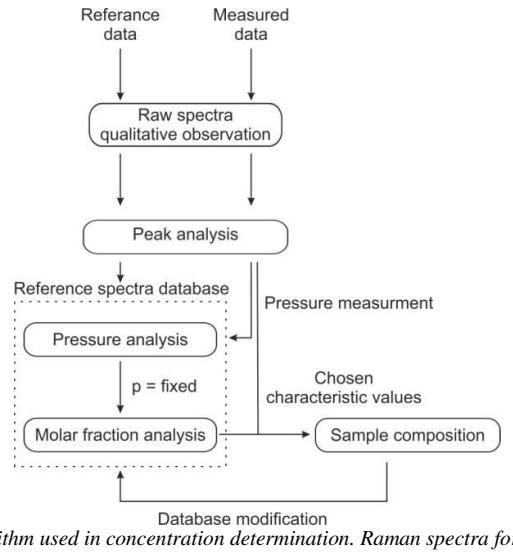

Fig. 2. Block diagram of an algorithm used in concentration determination. Raman spectra for a set of mixtures are collected for various pressures. Signals for a given element are Raman peak parameters such as position and area. These parameters' pressure behavior is reference spectra database. Analysis of parameters for the unknown sample under given pressure altogether with database allows composition calculation. PLS and Artificial Neural Network approach are two methods of the analysis presented in this paper.

The first is a construction of a database from measurements performed for mixtures with known composition. Here we will limit our analysis to the case of varying pressure, but a similar approach can be applied to varying temperatures. The second part is a module that calculates concentration for unknown sample based on the database. This step was performed using either the PLS method or an Artificial Neural Network. In the case of the PLS method approach, after the determination of a concentration, the database can be modified, i.e., data for samples with a composition significantly different than calculated one are excluded from the analysis. Further details will be given in the next chapters.

Real-time applications such as monitoring require the fast operation of the program. It should be noted that building a database is the most time-consuming part. Depending on the raw spectra number, this process can take 1 hour on a PC, but this procedure needs to be done only once. Further composition determination lasts shorter than a minute for both methods. Writing a dedicated application in a language such as C\# or C can further increase the speed of calculation.

Initial data processing

Each mixture was measured for several pressures. In Fig. 3 are shown spectra collected for a given sample under several pressures from 0.410 MPa to 2.835 MPa. The left label in Fig. 3 denotes the composition of the mixture measured by GC. The most prominent feature is a peak in a position 2917 cm^{-1}, corresponding to methane vibration. The inset shows an enlarged area of this peak. Determination of the influence of pressure on a single peak is the main objective for creating a database.

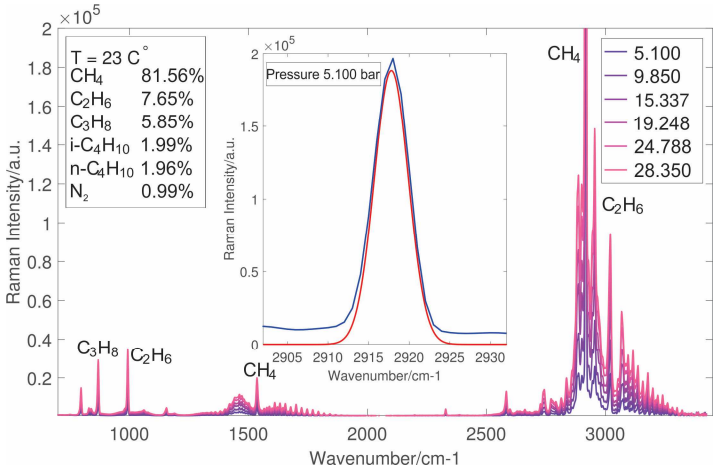

Fig. 3. Exemplary Raman spectra were collected for a gaseous mixture. The left table shows theoretical composition measured with GC. In the right table, pressures under which spectra were collected are shown (in MPa). The inset shows enlarged methane 2917 cm^{-1} peak. Increase and position shift is visible with a change of pressure. Characteristic peaks for other components are visible.

Peaks corresponding to vibrations for other components are marked. It should be noted that several bands can be visible for one component due to the presence of several types of vibration mods. For further analysis always only one band is taken into consideration. It is either the strongest one or a band that is separated from the other (lowest overlapping). Near methane 1534 cm^{-1} peak, one can see several smaller peaks, which are rovibrational lines of ν_2 band of methane. Their analysis is beyond the scope of this work.

As a model of a single peak, a Voight distribution can be adopted:

$$V(x,\sigma,\gamma) = \int_{-\infty}^{+\infty} G(x',\sigma)L(x-x',\gamma)dx$$

it is a convolution of Lorentzian and Gaussian distributions given by:

$$L(x,\gamma) = \frac{\gamma}{\pi(x^2+\gamma^2)}$$

where γ is a width of Lorentzian, and

$$G(x,\sigma) = \frac{e^{\frac{-x^2}{2\sigma^2}}}{\sigma\sqrt{2\pi}}$$

where σ is a width of Gaussian.

The first distribution is a natural shape of a characteristic Raman band, while the second corresponds to apparatus broadening.

The total width of a band is given by (Olivero, 1977):

$$f_v = 0.5246f_L + \sqrt{0.2166{f_L}^2 + {f_G}^2}$$

where $f_L = 2\gamma, f_G = 2\sigma\sqrt{2ln2}$.

In a practical approach, in the fitting procedure as starting values, there were given theoretical position, a width of Void distribution (that shape was set constant), height, and window width. During the fitting procedure, each parameter was adjusted to minimize the error function r^2. Widow width was adjusted for highest pressure and then set constant for lower pressures for a given sample. State of a program was written in the MATLAB environment. Peak fitting was performed with the use of the *peakfit* algorithm function (O'Haver, 2015).

The procedure also allows distinguishing real signals from noise. For the determination of the presence of a given element, logical conditions were added.

First, we imposed a constrain for signal-to-noise to the value 3:1. The signal-to-noise ratio was determined to form a formula (Blitz, 2002):

$$\boldsymbol{SNR} = \frac{\boldsymbol{I_P - I_B}}{\boldsymbol{\sigma_B^2}},$$

where I_P is peak intensity and I_B average background intensity over the chosen window and σ_B^2 the Root Mean Square (RMS) of the background.

Second, concentration was set to a 0 value if later determined fraction was smaller than 0.001. The exemplary fit of the model function is shown in the insert Fig. 3. The blue line denotes experimental data, while red is a fitted model function. It can be seen that chosen model function maps the characteristic signal. The only deviation occurs outside a characteristic band, i.e., in the background region. It can effects results for very low concentrations. Similar fitting is performed to all bands within spectra which corespondents to possible components and for each pressure. All bands for which fitting was performed are listed in Table 1.

The peak can be described by four numbers, i.e., the position of a band, its width, height, and area. In this work, we will limit the analysis only to the position and area which consists of the reference spectra database. Uncertainty of position determination is given by standard deviation of a mean, while for peak area A_P is equal to $\sqrt{A_P}$

Tab. 1 *List of characteristic bands which were analyzed for each spectrum*

Component	*Vibration*	*Wavenumber* [cm^{-1}]*
methane – CH_4	*C-H sym. stretching*	*2916*
ethane – C_2H_6	*C-C stretching*	*994*
propane – C_3H_8	*C-C stretching*	*870*
i-butane – i-C_4H_{10}	*C-C stretching*	*794*
n-butane – n-C_4H_{10}	*C-C stretching*	*827*
i-pentane – i-C_5H_{12}	*C-C stretching*	*764*
n-pentane – n-C_5H_{12}	*C-C stretching*	*401*
hexane – n-C_6H_{14}	*C-C stretching*	*893*
nitrogen – N_2	*N-N stretching*	*2330*

**position in ambient pressure*

Results

Pressure dependence

To obtain peak parameters, i.e., its wavenumber and area from the database for an arbitrary pressure, one must determine the functional relationship between those parameters and pressure. Exemplary experimental results for methane, ethane, and nitrogen band for spectra of a mixture shown in Fig. 3 are presented in Fig. 4. One can observe that the wavenumber is shifted towards lower values with an increase of pressure.

A ν_1 peak position changes from 2917.8 cm^{-1} for pressure 0.5 MPa to 2917.2 cm^{-1} for pressure 3 MPa. Similar behavior was shown in (Petrov 2017b), where ν_1 was shown to be linear up to pressure 55 bar where peak position was 2616.7 cm^{-1}. In the paper, we focused on the analysis of the strongest bands of each component. However, a similar analysis can be performed for other bands. In the (Petrov 2017b) was shown that methane ν_2 (1534 cm^{-1}) peak position increases with respect to pressure while $2\nu_2$ (3072 cm^{-1}) is decreasing with pressure, but this trend is non-linear. It was shown that for above 25 MPa $\nu_{1,\ the}$ peak position changes non-linearly (Hansen 2001b). In particular, an above 100 MPa increase of the peak position is observed. Figure 4 shows a linear increase of peak area with pressure. It should be noted that slopes are different for each component; therefore, relative peak intensity changes with pressure. Similarly, linear intensity increase was shown in (Petrov 2017a) for O_2 and N_2, while in the case of CO_2 vibrational bands, that effect is non-linear. In (Seitz 1993) was shown an increase of CH_4 and N_2 in the function of density. Relative intensities ratio changes with pressure were shown for CH_4 and N_2 mixture in (Seitz 1993). The CH_4/ N_2 ratio incenses to pressure 10 MPa while for higher remain constant. That shows the following assumption of linear area and peak position changes are not valid for pressures higher than 10 MPa or mixture with CO_2. Therefore, presented trends cannot be extrapolated for higher pressures. In that case, for higher pressures, a new database has to be collected, and a new model determined.

Presented changes of position and area can be approximate by a straight line determined utilizing a PLS of a form:

$$\boldsymbol{y_{ij}^k = b_{ij}^k p + a_{ij}^k}$$

where k denotes parameter (wavenumber or area), j band, i sample, and p pressure. By determining coefficients b_{ij}^k and a_{ij}^k we can calculate the value of a given parameter y_{ij} for an arbitrary pressure p.

Parameters y_{ij}^k calculated for each band for all samples are the input for the concentration determination for both the PLS and Neural Network methods.

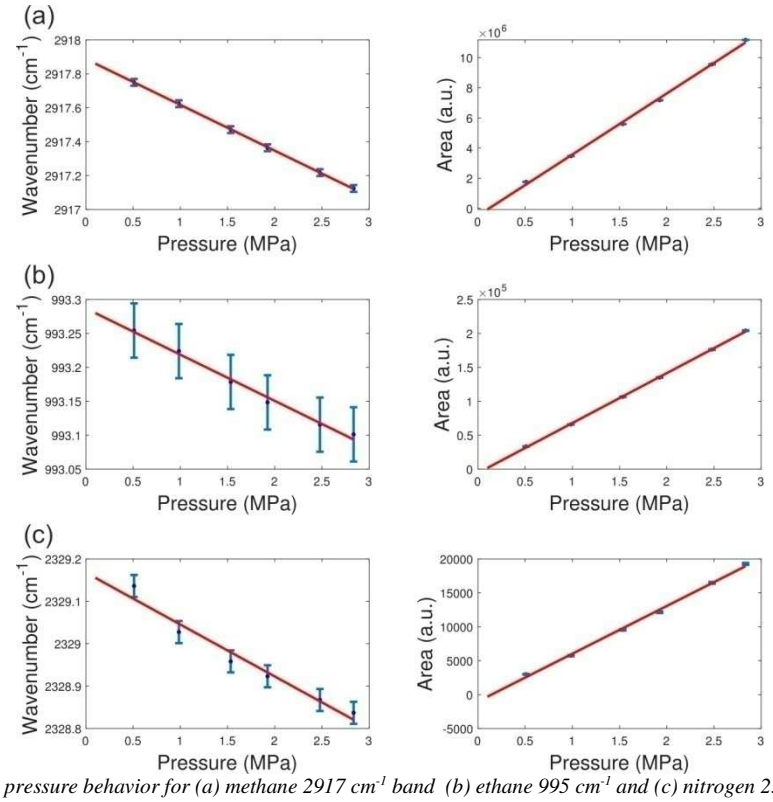

Fig. 4. Exemplary pressure behavior for (a) methane 2917 cm^{-1} band (b) ethane 995 cm^{-1} and (c) nitrogen 2330 cm^{-1} band. Left panels show wavenumber while right area behavior. A solid red line is a PLS trend fitted to experimental data. Parameters obtained from spectra are shown in Fig. 3.

Partial least squares regression analysis

In this part of the analysis, we determine a relation between parameters y_{ij}^{k} calculated for a given pressure and concentration of component j. Fig. 5 shows the relation between wavenumber and peak area under pressure 1 MPa for each sample i. Results are shown for methane, ethane, and nitrogen band. It should be stressed that each point corresponds to a different reference mixture in this case.

The most evident feature for a wavenumber behavior is the lack of certain relationships with a concentration of a given component. This shows that wavenumber depends not only on the pressure of the sample and concentration of a given element but also is sensitive for a fraction of other components. Previous studies of binary samples show similar behavior. In (Seitz 1993) was shown the impact of composition changes for CH_4, N_2 mixture. An increase of CH_4 fraction results in a decrease of peak position, while an increase of N_2 concentration results in an increase of peak position. Two CH_4-C_2H_6 mixtures were analyzed by (Hansen 2001). It was shown that higher C_2H_6 concentration results in a higher decrease of methane ν_1 peak position. The impact of the environment on the methane ν_1 position was discussed by (Petrov 2019). CH_4-CO, CH_4- CO_2, CH_4-H_2 were studied. It was shown that the impact on the environment is stronger with increasing pressure. In that system higher concentration of the second component resulted in smaller methane ν_1 peak position change. It is the opposite of the C_2H_6 impact. Therefore, in the case of a multi-component environment, its impact on a given peak position is vague.

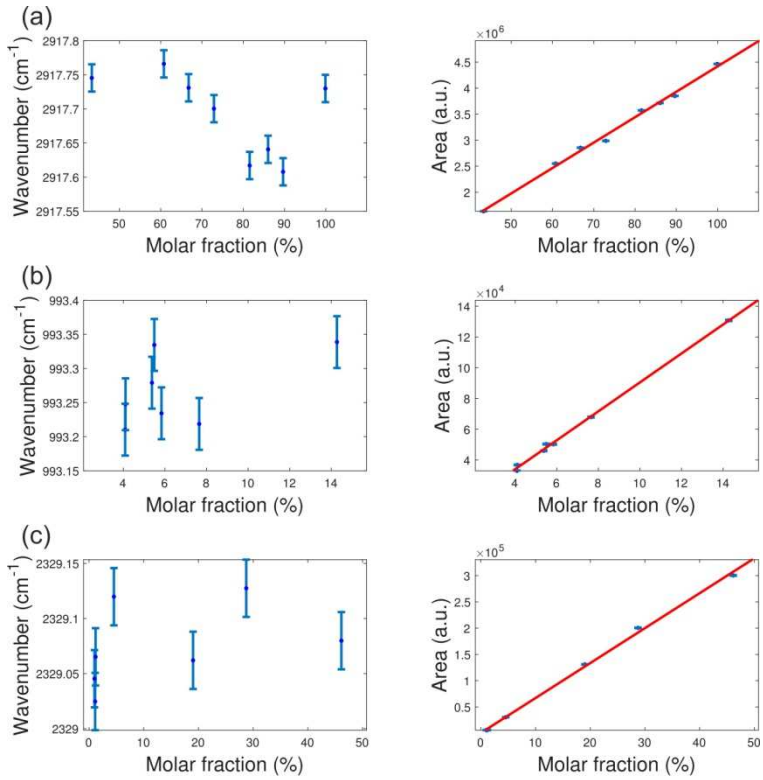

Fig. 5. Peak parameters' relation with respect to the molar fraction of given element under pressure 1 MPa. Values for (a) methane, (b) ethane, (c) nitrogen. Left panels show position while right area behavior. The solid red line is a fitted trend. In the case of area, relations can be treated as linear. In contrast for a position, behavior concerning a molar fraction change is non-linear.

In contrast, the area changes linearly with concentration. This means that area of a given peak depends solely on the pressure and concentration of a given component. Similar linear relation of peak area, as shown in Figure 4, was determined for methane, ethane, and propane (Sharma 2016). In this work 4 mixtures containing with concentrations varied between 77.50-81.40% for C_2H_6, 10.22-7.99% for C_3H_8, 2.41-1.41% for i-C_4H_{10}, 2.26-0.99% for n- C_4H_{10} and 2.90-3.01% for N_2.

Therefore, concentration can be successfully resolved with a PLS approach. Wavenumber analysis can be perspective when one has to distinguish between two fluid that differs in concentration only significantly. This is especially important for a reservoir fluid analysis because a small change of heavier hydrocarbon concentration can significantly impact their thermodynamic properties, such as dew point (Elsharkawy, 2002). The effect of wavenumber shift connected with concentration has been studied for binary systems (Petrov, 2019). In the case of the multi-component system, such behavior is strongly non-linear. Since our data are limited, we cannot determine such a relation analytically but can employ ANNs that can take this effect into account.

To calculate composition for any sample based on the PLS method, we have to determine coefficients of an equation:

$$\boldsymbol{Y_{ij}^k = A_j^k x_j + B_j^k}$$

where x is a molar fraction of a component j. We determine coefficients A_j^k, B_j^k. For the sample with an unknown concentration, we can measure the value $Y_{exp,j}^k$ and by solving the previous equation with respect to concentration x_j we can calculate the fraction of each component within this sample

$$\boldsymbol{x_j = \frac{Y_{exp,j}^k - B_j^k}{A_j^k}}$$

This approach also allows one to estimate the molar fraction of components present in the sample but were not detected in the spectra, such as higher hydrocarbons C7+, hydrogen sulfide, etc. The total remnant fraction is given by $1 - \sum_j x_j$. This kind of information can show the necessity of the extension of a band set. It can be especially important for field measurements. A free model can also be helpful to point out possible peak overlapping. The overlapping can give rise to peak intensities resulting in the overestimation of concentration. This result is total compositions that will exceed 100%.

If we assume that all components within a sample were detected, we can impose a normalization condition:

$$x_{j,norm} = \frac{Y^k_{exp,j} - B^k_j}{A^k_j \sum_j \frac{Y^k_{exp,j} - B^k_j}{A^k_j}}$$

This approach ensures better results in the case of a beam attenuation or laser drift which can take place during on-field measurements caused by weather conditions. The linear method allows determining fraction uncertainty. The standard deviation of area $\delta Y^k_{exp,j}$ is given by $\sqrt{Y^k_{exp,j}}$ error propagation can be calculated from:

$$\delta_{x_j} = \sqrt{\left(\frac{1}{A^k_j}\right)^2 \left(Y^k_{exp,j}\right)^2 + \left(\frac{-1}{A^k_j}\right)^2 \delta^2_{B^k_j} + \left(\frac{Y^k_{ij} - B^k_j}{\left(A^k_j\right)^2}\right)^2 \delta^2_{A^k_j}}$$

Neural network analysis

For a gas composition determination, we used a multi-layer feedforward neural network. It consists of three layers:

- input layer
- single hidden layer
- output layer

The topology of the network is shown in Fig. 6. In the case of composition determination based on the area of peaks, there was one input neuron responsible for an area of the element. In a hidden layer were 2400 neurons. Neuron from the input layer was connected to every neuron from the hidden layer. The activation function was a hyperbolic tangent activation function. The learning algorithm was L-BFGS-B (limited-memory Broyden-Shanno bounded algorithm) (Byrd, 1995).

Weights w^I_n, w^H_m are determined in a learning process.

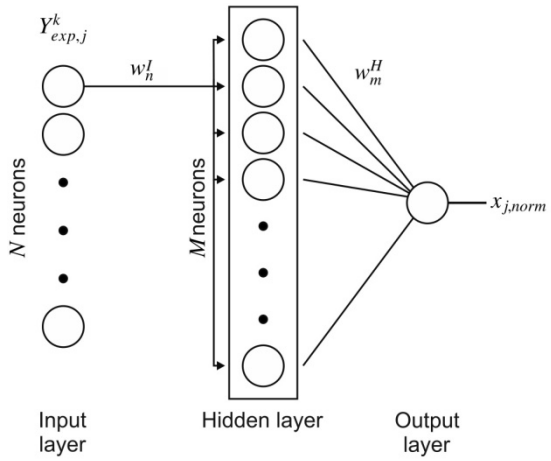

Fig. 6. Topology of the used Artificial Neural Network. The input layer consists of N and hidden layer M neurons. Every neuron from an input layer is connected with each neuron from the hidden layer and transfers the same signal given by a weight function w^I_n. The output layer consists of a single neuron connected with every neuron from the hidden layer. As an output, this neuron gives a number $x_{j,norm}$. The signal from a hidden layer to an output neuron is determined by a weight function w^H_m.

The database was divided randomly into two sets: 80 % of data is a learning set, and 20 % is a testing set. Then learning procedure was repeated till results given for a test set were satisfying, i.e., their deviations from concentrations obtained for GC were smaller than assumed accuracy, or the number of repetitions exceeds a specified number of iterations.

For a determination of concentration based on both area and shifts, there were two neurons in the input layer and 600 neurons in a hidden layer. A ReLu (Rectified Linear Unit) activation function was used. The learning algorithm was Adam (Kinga, 2015).

It should be marked that since the learning dataset is taken randomly as well as initial wights values are random output networks are different from one experiment to another. Both the structure of the network (the number of neurons), the activation function, and the learning algorithm were selected experimentally based on the results for the validation set. The different structure of the network in both considered cases results from the

difference in the training data sets (the second set is larger and contains, apart from the intensity, also the shifts). Above mentioned issues are the main disadvantages from the point of view of repeatability of measurement.

Molar fraction determination for a reference sample

The feasibility of the proposed method was shown by the determination of a molar fraction for one of a sample within a measured data set. First, this sample was removed from the spectra database. Coefficients Y_{ij}^{k} were therefore determined based on other samples. These samples consist of various concentrations of hydrocarbons from methane to n-butane and nitrogen. Since we did not have samples with i-pentane, n-pentane, or hexane in the reference spectra database, we are unable to determine the concentration of those components quantitatively. However, the algorithm still gives information if the given component is present within the measured sample or not.

The algorithm allows to performance of the analysis for any arbitrarily chosen pressure. Here will be shown results for 1 MPa. We compare results with gas chromatography (GC). It should be pointed out that GC measurements were performed in ambient pressure. First, compositions were calculated using the PLS method without normalization (Free Model) and later normalized. Second, we show results from the neural network approach based solely on peak intensities (ANN+i) and with the network which takes into account both intensities and peak positions (ANN+is).

The calculated composition for the first pressure is shown in Table 2. The algorithm has detected components up to n-butane based on bands listed in Table 1. It also showed which components are not present within this sample. One can see that for a methane fraction, the free model gives a value slightly higher than theoretical one relative error is if the order of 1.4 %. The procedure of normalization reduces this value to 0.5 %. The highest disagreement takes place for nitrogen and n-butane, where the relative error is equal to 21 % and 5 % for a free model. After normalization, we obtain values of 22 % and 5 %, respectively. For other components, errors do not exceed 3 %.

Methane molar fraction determined by Neural Network based on solely intensities is higher than for the GC value while for network based on both intensities and positions lower. The relative error for both networks is lower than the error obtained for the PLS method, i.e., 0.3 % and 0.15 %. However, the biggest improvement of results one can observe is the case of nitrogen. For the first network (ANN+i) error is 10.2 % and while 1.1 % is for the second network (ANN+is). There is no significant change in uncertainty for other components between ANNs approaches.

Tab. 2 *Concentrations for a test sample for a pressure 1 MPa. Analysis was performed using gas chromatography (GC), PLS method (free model and with normalization), and Artificial Neural Networks (ANN)*

Line	*GC*	*Free Model*	*Norm.*	*ANN+i*	*ANN+is*
CH_4	*0.8156(2)*	*0.8269(2)*	*0.8193(2)*	*0.8180*	*0.8144*
C_2H_6	*0.0765(2)*	*0.0760(3)*	*0.0754(3)*	*0.0751*	*0.0771*
C_3H_8	*0.0585(2)*	*0.0599(2)*	*0.0594(2)*	*0.0597*	*0.0591*
$i\text{-}C_4H_{10}$	*0.0199(1)*	*0.0196(1)*	*0.0194(1)*	*0.0196*	*0.0204*
$n\text{-}C_4H_{10}$	*0.0196(1)*	*0.0188(1)*	*0.0187(1)*	*0.0187*	*0.0190*
$i\text{-}C_5H_{12}$	*0.0000*	-	-	-	-
$n\text{-}C_5H_{12}$	*0.0000*	-	-	-	-
C_6H_{14}	*0.0000*	-	-	-	-
N_2	*0.0099(1)*	*0.0079(1)*	*0.0078(1)*	*0.0089*	*0.0100*

The analysis shows that both methods are feasible to determine the composition; however, we obtain a relatively high error for nitrogen. This error can be reduced by using a neural network considering both peak areas and positions. It should be noted that although the range of the shift variability is small, this value may have a significant impact on the output data, which results directly from the weight values determined. Due to the extensive structure of the network (hidden layer with 600 neurons), the relationship between the peak shift and the component concentration cannot be determined directly.

Based on the compositions shown in Table 2, we calculated thermodynamic properties such as Wobbe index, higher and lower heating value, and density. Properties were calculated according to (ISO6976, 2016) and are shown in Table 3. Properties obtained utilizing Raman spectroscopy are in good agreement with GC. Wobbe index calculated based on PLS differs from Wobbe index from GC by 0.2 %. Wobbe index from ANN+i differ by 0.04 % and form ANN+is by 0.02 % while comparing to GC. The heating value-form PLS differs by 0.07 %, ANN values differ by 0.09 % from the GC result. Significantly higher are errors of density. For regression error is 0.4 %, for ANN+i is 0.3 % and for ANN+is is 0.2 %.

Tab. 3 *Comparison of selected thermodynamic properties obtained for a test sample at pressure 1 MPa*

Property	*GC*	*Free Model*	*Norm.*	*ANN+i*	*ANN+is*
Wobbe index [MJ/m^3]	*54.87(3)*	*54.88(3)*	*54.87(3)*	*54.87*	*54.72*
Higher heating value [MJ/m^3]	*46.27(3)*	*46.19(3)*	*46.18(3)*	*46.23*	*46.11*
Lower heating value [MJ/m^3]	*41.95(3)*	*41.87(3)*	*41.87(3)*	*41.91*	*41.80*
Density [kg/m^3]	*0.8716(4)*	*0.8682(4)*	*0.8681(4)*	*0.8698*	*0.8701*

Gas separator system monitoring

The last part was to show the possibility of determining a composition for gas flow in industrial applications. Constructed setup was placed at a separation system installed on a natural gas well Wysin-3H in northern Poland. Well, the head outflow was connected with a 2" pipe to a mobile three-phase separator. Raman probe was mounted to a gas outflow with 1/2" NPT spigot. The scheme of the setup is shown in Fig. 7. The pressure of the measured gas was 0.452 MPa, and the air temperature was 8°C. In-situ measurement temperature was lower than the temperature in which reference spectra were collected, equal to 23°C. Collected spectra were processed with both the PLS method and neural network algorithm based on peak areas presented in previous chapters. For results validation, gas was sampled and measured on a gas chromatograph. Firstly, this experiment's network, which calculates compositions based on both areas and positions, did not give satisfactory results. It is caused by a significant shift of spectra connected with the impact of temperature on the molecule's vibration as well as the impact on the spectrometer itself. Since temperature behavior was beyond the scope of this study, we are unable to perform temperature correction. Results are presented in Table 4.

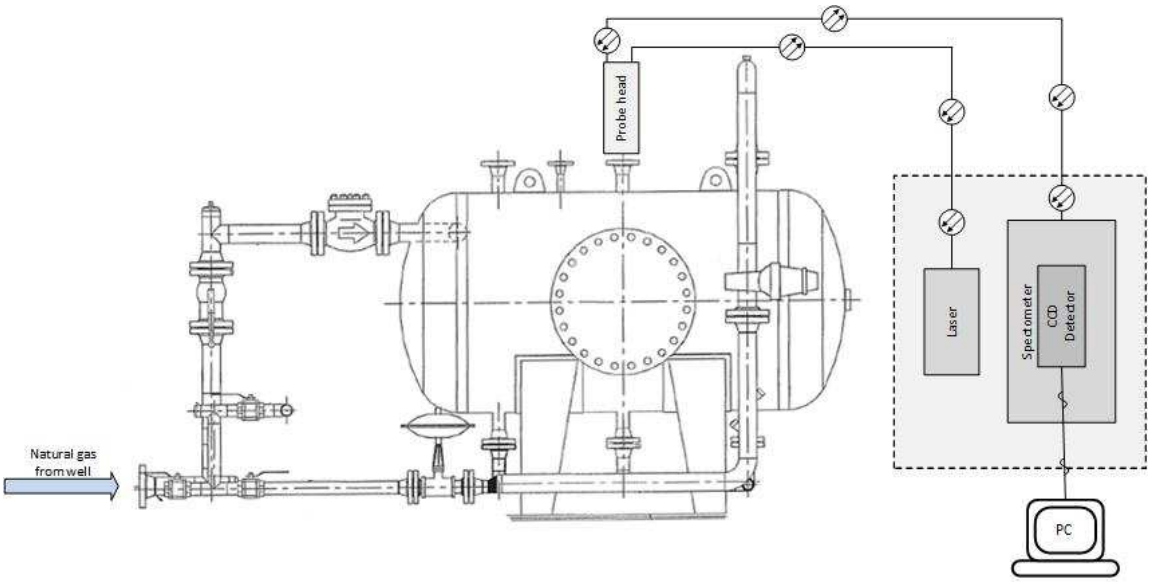

Fig. 7. Scheme of a mounting of a current Raman system to a three-phase gas separation system. Reservoir fluid flows from a wellhead to a separator. Composition is determined by a Raman spectrometer at the gas vent line. For sampling Raman probe was removed from a gas flow to a sampler.

Firstly, due to limited reference spectra, Raman analysis was unable to detect hydrocarbons heavier than butanes as well as carbon dioxide. However, the free model allows us to estimate not detected fraction for a value 0.0157, while a gas chromatography gives a fraction of hydrocarbons heavier than butanes and carbon dioxide equal to 0.0066. Relative uncertainty for methane is 1.1 % for a free model, 2.6 % after normalization, and 1.5 % for the neural network. We can see that propane and i-butane uncertainties are relatively high. For both PLS method approaches is above 26 % for a network above 14 %. In the case of i-butane for each method, uncertainties exceed 50 %. This disagreement can be connected, with mentioned above, temperature impact as well as possible liquid phase occurrence in a fluid.

This significantly impacts thermodynamic properties disagreement between the GC and Raman approach. Thermodynamic properties for natural gas samples were calculated in the same manner as for the test sample. Results are shown in Table 5. The Wobbe index error is 1.5 % for PLS and 1 % for ANN, while heating values differ by 3.5 % for PLS and 3 % for ANN form GC value. Density error is 4.5 % and 3.5 % for PLS and ANN.

Tab. 4 *Concentrations for a gas flow from separator on gas production well Wysin-3H. Gas pressure 0.452 MPa. Analysis was performed using gas chromatography (GC), PLS method (free model and with normalization), and Artificial Neural Network (ANN+i)*

Line	*GC*	*Free Model*	*Norm.*	*ANN+i*
CH_4	*0.8573(2)*	*0.8660(5)*	*0.8798(5)*	*0.8705*
C_2H_6	*0.0829(2)*	*0.0812(3)*	*0.0825(3)*	*0.0849*
C_3H_8	*0.0296(1)*	*0.0215(2)*	*0.0219(1)*	*0.0252*
$i\text{-}C_4H_{10}$	*0.0088(1)*	*0.0035(1)*	*0.0036(1)*	*0.0040*
$n\text{-}C_4H_{10}$	*0.0047(1)*	*0.0044(1)*	*0.0044(1)*	*0.0055*
$i\text{-}C_5H_{12}$	*0.0023(1)*	-	-	-
$n\text{-}C_5H_{12}$	*0.0020(1)*	-	-	-
C_6H_{14}	*0.0012(1)*	-	-	-
N_2	*0.0101(1)*	*0.0077(1)*	*0.0078(1)*	*0.0100*
CO_2	*0.0011(1)*	-	-	-

Tab. 5 *Comparison of selected thermodynamic properties obtained for a gas flow from separator on gas production well Wysin-3H. Gas pressure 0.452 MPa*

Property	*GC*	*Free Model*	*Norm.*	*ANN+i*
Wobbe index [MJ/m^3]	*53.17(3)*	*52.56(4)*	*52.57(4)*	*52.63*
Higher heating value [MJ/m^3]	*43.21(3)*	*41.77(4)*	*41.77(4)*	*42.07*
Lower heating value [MJ/m^3]	*39.10(3)*	*37.74(4)*	*37.75(4)*	*38.03*
Density [kg/m^3]	*0.8094(4)*	*0.7736(5)*	*0.7737(5)*	*0.7828*

Conclusions

In this paper, we showed the procedure for the determination of gas composition with Raman spectroscopy. The first part is the construction of a proper database. The database has to contain the appropriate number of test samples measured in several pressures. However, the minimal number of required data is not clearly defined. It is especially important for a neural network.

Information connected with composition can be retrieved from the Raman spectrum in many ways, here we decided to analyze the area and position of a given characteristic peak. We determined an influence of pressure which allowed us to propose a useful experimental tool capable of carrying on measurements for any pressure also for extrapolated pressure analysis is possible. Similar analysis can also be conducted for temperature, which can further be extended application to high-temperature, high-pressure processes.

The first conclusion from the analysis is that the composition can be calculated based on the area by utilizing the PLS method. Adaptation of neural networks allows extending the analysis to positions of peaks.

We proposed and compared these two methods of composition determination. Both gave satisfying results for a test sample, but the ANN is in better agreement with the composition obtained from a GC. in the case of separator measurements, results have relatively large uncertainties. Disagreements and be connected with a temperature influence and fluid liquefaction. The use of 105 m fiberoptic in perspective can be allowed to conduct measurements for industrial processes such as flow in pipelines exhaust gas analysis. The particular adaptation of longer fiber can expand possible applications for downhole composition determination for both conventional and unconventional gas reservoirs such as shales and coalbed methane. The system is not limited to gas measurement; it is capable of also performing measurements of liquid. The most perspective is a returning drilling mud quality assessment in this case.

Extension of the database for a temperature impact on spectra can bring significant improvement in the case of the gas separator when the temperature is different when compared to laboratory experiments. However, in multi-component samples, one needs to calculate density based on real gas equations such as GERG-2008 or SRK; they need apriori knowledge about sample composition. In this kind of experiment, stabilization of temperature is the most long-lasting part of the analysis. In estimate, 1 hour is needed to reach a given temperature, and stabilization of the system requires 1-2 hours what significantly extends measurements.

References

Al-Fattah, S. M., Startzman, R. A., & others. (2001). Predicting natural gas production using artificial neural network. *SPE Hydrocarbon Economics and Evaluation Symposium.*

Al-Marhoun, M. A., Ali, S. S., Abdulraheem, A., Nizamuddin, S., & Muhammadain, A. (2014). Prediction of Bubble Point Pressure From Composition of Black Oils Using Artificial Neural Network. *Petroleum Science and Technology, 32*, 1720–1728.

Al-Sirri, D., Gharbi, R. C., & others. (2011). Predicting Lower Fars Heavy Oil Molar Compositions Using Artificial Neural Networks. *SPE Heavy Oil Conference and Exhibition.*

APIRP44. (2004). *Sampling Petroleum Reservoir Fluids, 2nd Ed.* American Petroleum Institute. American Petroleum Institute.

Bowley, H. J., Gerrard, D. L., Louden, J. D., & Turrell, G. (2012). *Practical Raman spectroscopy.* Springer Science & Business Media.

Bērziņš, K., Fraser-Miller, S. J., & Gordon, K. C. (2020). Recent Advances in Low-Frequency Raman Spectroscopy for Pharmaceutical Applications. International Journal of Pharmaceutics, 120034.

Beyssac, O. (2020). New trends in Raman spectroscopy: from high-resolution geochemistry to planetary exploration. Elements: An International Magazine of Mineralogy, Geochemistry, and Petrology, 16(2), 117-122.

Blitz, J. P., & Klarup, D. G. (2002). Signal-to-noise ratio, signal processing, and spectral information in the instrumental analysis laboratory. Journal of chemical education, 79(11), 1358.

Briones, M. F., Rojas, G. A., & others. (1994). Application of neural networks in the prediction of reservoir hydrocarbon mixture composition from production data. *SPE Annual Technical Conference and Exhibition.*

Bryndzia, L. T., Braunsdorf, N. R., Hofmann, R., Morgan, Q., Christian, P., Toews, A., et al. (2016). Down-Hole Reservoir Raman System: A Novel New Technology for the Rapid Appraisal of Shale Gas Resource Potential. *Unconventional Resources Technology Conference, San Antonio, Texas, 1-3 August 2016*, (pp. 409–425).

Buldakov, M. A., Korolev, B. V., Matrosov, I. I., Petrov, D. V., & Tikhomirov, A. A. (2013). Raman gas analyzer for determining the composition of natural gas. *Journal of Applied Spectroscopy, 80*, 124–128.

Buldakov, M. A., Matrosov, I. I., Petrov, D. V., & Tikhomirov, A. A. (2012). Raman gas-analyzer for analyzing environmental and technogenic gas media. *Atmospheric and Oceanic Optics, 25*, 298–303.

Byrd, R. H., Lu, P., Nocedal, J., & Zhu, C. (1995). A limited memory algorithm for bound constrained optimization. *SIAM Journal on Scientific Computing, 16*, 1190–1208.

Dąbrowski, K. M., Kuczyński, S., Barbacki, J., Włodek, T., Smulski, R., & Nagy, S. (2019). Downhole measurements and determination of natural gas composition using Raman spectroscopy. *Journal of Natural Gas Science and Engineering, 65*, 25-31.

Dąbrowski, K., Kuczyński, S., Włodek, T., Smulski, R., & Barbacki, J. (2018). Characterization of natural gas by Raman spectroscopy and its application for in-situ measurements. *AGH Drilling, Oil, Gas, 35*, 125–138.

De Beer, T., Burggraeve, A., Fonteyne, M., Saerens, L., Remon, J. P., & Vervaet, C. (2011). Near-infrared and Raman spectroscopy for the in-process monitoring of pharmaceutical production processes. International journal of pharmaceutics, 417(1-2), 32-47.

Eichmann, S. C., Kiefer, J., Benz, J., Kempf, T., Leipertz, A., & Seeger, T. (2014). Determination of gas composition in a biogas plant using a Raman-based sensor system. *Measurement Science and Technology , 25*, 075503.

Elsharkawy, A. M. (2002). Predicting the dew point pressure for gas condensate reservoirs: empirical models and equations of state. *Fluid Phase Equilibria, 193*, 147–165.

Frosch, T., Meyer, T., Schmitt, M., & Popp, J. (2007). Device for Raman difference spectroscopy. *Analytical chemistry, 79*, 6159–6166.

Goodacre, R., Neal, M. J., & Kell, D. B. (1994). Rapid and quantitative analysis of the pyrolysis mass spectra of complex binary and tertiary mixtures using multivariate calibration and artificial neural networks. *Analytical Chemistry, 66*, 1070–1085.

Halvorson, R. A., & Vikesland, P. J. (2010). Surface-enhanced Raman spectroscopy (SERS) for environmental analyses, ACS Publications.

Hansen, S. B., Berg, R. W., & Stenby, E. H. (2001). High-pressure measuring cell for Raman spectroscopic studies of natural gas. *Applied Spectroscopy, 55*, 55–60.

Hansen, S. B., Berg, R. W., & Stenby, E. H. (2001). Raman spectroscopic studies of methane—ethane mixtures as a function of pressure. *Applied Spectroscopy, 55*, 745–749.

Hansen, S. B., Berg, R. W., & Stenby, E. H. (2000). *The application of Raman spectroscopy for analysis of multi-component systems.* Ph.D. dissertation, Technical University of DenmarkDanmarks Tekniske Universitet, Department of ChemistryInstitut for Kemi.

Hegeman, P. S., Dong, C., Varotsis, N., Gaganis, V., & others. (2009). Application of artificial neural networks to downhole fluid analysis. *SPE Reservoir Evaluation & Engineering, 12*, 8–13.

Hippler, M. (2015). Cavity-enhanced Raman spectroscopy of natural gas with optical feedback CW-diode lasers. Analytical Chemistry, 87(15), 7803-7809.

Gautam, Rekha, et al. "Review of multidimensional data processing approaches for Raman and infrared spectroscopy." EPJ Techniques and Instrumentation 2.1 (2015): 1-38.

ISO. (2016). *6976:2016, Natural gas — Calculation of calorific values, density, relative density, and Wobbe indices from the composition.* International Organization for Standardization. International Organization for Standardization.

Keiner, R., Frosch, T., Massad, T., Trumbore, S., & Popp, J. (2014). Enhanced Raman multigas sensing–a novel tool for control and analysis of 13 CO 2 labeling experiments in environmental research. Analyst, 139(16), 3879-3884.

Kiefer, J. (2015). Recent advances in the characterization of gaseous and liquid fuels by vibrational spectroscopy. *Energies, 8*, 3165–3197.

Kiefer, J., Obert, K., Bösmann, A., Seeger, T., Wasserscheid, P., & Leipertz, A. (2008). Quantitative Analysis of Alpha-D-glucose in an Ionic Liquid by Using Infrared Spectroscopy. *ChemPhysChem , 9*, 1317–1322.

Kiefer, J., Seeger, T., Steuer, S., Schorsch, S., Weikl, M. C., & Leipertz, A. (2008). Design and characterization of a Raman-scattering-based sensor system for temporally resolved gas analysis and its application in a gas turbine power plant. *Measurement Science and Technology, 19*, 085408.

Kinga, D., & Adam, J. B. (2015). A method for stochastic optimization. *International Conference on Learning Representations (ICLR)*, *5.*

Korjani, M. M., Popa, A. S., Grijalva, E., Cassidy, S., Ershaghi, I., & others. (2016). Reservoir Characterization Using Fuzzy Kriging and Deep Learning Neural Networks. *SPE Annual Technical Conference and Exhibition.*

Kuczyński, S., Włodek, T., Smulski, R., Dąbrowski, K., Krakowiak, M., Barbacki, J., et al. (2017). Application of Raman spectroscopy analysis in unconventional natural gas reservoirs–density and pressure dependence on Raman signal intensity. *AGH Drilling, Oil, Gas, 34*, 761-774.

Kutner, M. H., Nachtsheim, C., & Neter, J. (2004). *Applied linear regression models.* McGraw-Hill/Irwin.

Lee, Loong Chuen, Choong-Yeun Liong, and Abdul Aziz Jemain. "Partial least squares-discriminant analysis (PLS-DA) for classification of high-dimensional (HD) data: a review of contemporary practice strategies and knowledge gaps." Analyst 143.15 (2018): 3526-3539.

Lippmann, R. (1987). An introduction to computing with neural nets. *IEEE Assp magazine, 4*, 4–22.

Long, D. A. (2002). The Raman effect: a unified treatment of the theory of Raman scattering by molecules. *West Sussex*.

MacDonald, S., & others. (2007). Measuring CO2 in Coalbed Reservoirs. *Rocky Mountain Oil & Gas Technology Symposium.*

Montgomery, D. C., Peck, E. A., & Vining, G. G. (2012). *Introduction to linear regression analysis* (Vol. 821). John Wiley & Sons.

O'Haver, T. (2015). Peak Finding and measurement, version 2 http://terpconnect. umd. edu/ toh/spectrum. *PeakFindingandMeasurement.htm* .

Olivero, J. J., & Longbothum, R. L. (1977). Empirical fits to the Voigt line width: A brief review. *Journal of Quantitative Spectroscopy and Radiative Transfer, 17*, 233–236.

Özbalci, B., Boyaci, İ. H., Topcu, A., Kadılar, C., & Tamer, U. (2013). Rapid analysis of sugars in honey by processing Raman spectrum using chemometric methods and artificial neural networks. *Food Chemistry, 136*, 1444-1452.

Özmen, A., Tekce, F., Ebeoğlu, M. A., Taşaltın, C., & Öztürk, Z. Z. (2006). Finding the composition of gas mixtures by a phthalocyanine-coated QCM sensor array and an artificial neural network. *Sensors and Actuators B: Chemical, 115*, 450–454.

Pan, Liangrui, et al. "A review of artificial intelligence methods combined with Raman spectroscopy to identify the composition of substances." arXiv preprint arXiv:2104.04599 (2021).

Petrov, D. V., & Matrosov, I. I. (2017). Pressure dependence of the Raman signal intensity in high-pressure gases. *Journal of Raman Spectroscopy, 48*, 474–478.

Petrov, D. V., & Matrosov, I. I. (2016). Raman Gas Analyzer (RGA): Natural Gas Measurements. *Applied spectroscopy, 70*, 1770–1776.

Petrov, D. V., Matrosov, I. I., Zaripov, A. R., & Maznoy, A. S. (2019). Effects of pressure and composition on Raman spectra of CO-H2-CO2-CH4 mixtures. *Spectrochimica Acta Part A: Molecular and Biomolecular Spectroscopy*.

Petrov, Dmitry V. "Pressure dependence of peak positions, half widths, and peak intensities of methane Raman bands (ν2, 2ν4, ν1, ν3, and 2ν2)." *Journal of Raman Spectroscopy* 48.11 (2017): 1426-1430.

Ranjan, A., Verma, S., Singh, Y., & others. (2015). Gas lift optimization using artificial neural network. *SPE Middle East Oil & Gas Show and Conference.*

Sandfort, V., Trabold, B. M., Abdolvand, A., Bolwien, C., Russell, P. S. J., Wöllenstein, J., & Palzer, S. (2017). Monitoring the Wobbe index of natural gas using fiber-enhanced Raman spectroscopy. Sensors, 17(12), 2714

Seitz, Jeffery C., Jill Dill Pasteris, and I-Ming Chou. "Raman spectroscopic characterization of gas mixtures; I, Quantitative composition and pressure determination of CH 4, N 2 and their mixtures." American Journal of Science 293.4 (1993): 297-321.

Shang, L., Chou, I., Burruss, R. C., Hu, R., Bi, X., & others. (2014). Raman spectroscopic characterization of CH4 density over a wide range of temperature and pressure. *Journal of Raman Spectroscopy, 45*, 696–702.

Sharma, Rachit, et al. "Raman analyzer for sensitive natural gas composition analysis." Optical Engineering 55.10 (2016): 104103.

Sieburg, A., Schneider, S., Yan, D., Popp, J., & Frosch, T. (2018). Monitoring of gas composition in a laboratory biogas plant using cavity-enhanced Raman spectroscopy. *Analyst, 143*, 1358–1366.

Sieburg, A., Knebl, A., Jacob, J. M., & Frosch, T. (2019). Characterization of fuel gases with fiber-enhanced Raman spectroscopy. Analytical and bioanalytical chemistry, 411(28), 7399-7408.

Włodek, T., Kuczyński, S., Smulski, R., & Polański, K. (2016). An application of a Raman scattering analyzer for the determination of natural gas composition at a processing plant. *AGH Drilling, Oil, Gas, 33*, 619.

Zuas, O., & Budiman, H. (2016). Estimating precision and accuracy of GC-TCD method for carbon dioxide, propane, and carbon monoxide determination at a different flow rate of carrier gas. Hemijska industrial, 70(4), 451-459.

Zubarev, D. I., & others. (2009). Pros and cons of applying proxy models as a substitute for full reservoir simulations. *SPE Annual Technical Conference and Exhibition.*